ACS NANO

www.acsnano.org

ARTICLE

Nanowire Magnetoscope Reveals a Cellular Torque with Left–Right Bias

Wei Liu,[†] Yuanye Bao,[†] Miu Ling Lam,[‡,§,∥] Ting Xu,[†] Kai Xie,[†] Hin Sum Man,[†] Edward Y. Chan,[†] Ninghao Zhu,[†] Raymond H. W. Lam,[†,§,∥] and Ting-Hsuan Chen*[,†,‡,§,∥]

[†]Department of Mechanical and Biomedical Engineering, [‡]School of Creative Media, [§]Centre for Robotics and Automation, City University of Hong Kong, Hong Kong Special Administrative Region

[∥]CityU Shenzhen Research Institute, Shenzhen, 518057, China

Supporting Information

ABSTRACT: **Cellular force regulates many types of cell mechanics and the associated physiological behaviors. Recent evidence suggested that cell motion with left–right (LR) bias may be the origin of LR asymmetry in tissue architecture. As actomyosin activity was found essential in the process, it predicts a type of cellular force that coordinates the development of LR asymmetry in tissue formation. However, due to the lack of appropriate platform, cellular force with LR bias has not yet been found. Here we report a nanowire magnetoscope that reveals a rotating force—torque—exerted by cells. Ferromagnetic nanowires were deposited and internalized by micropatterned cells. Within a uniform, horizontal magnetic field, the nanowires that initially aligned with the magnetic field were subsequently rotated due to the cellular torque. We found that the torque is LR-biased depending on cell types. While NIH 3T3 fibroblasts and human vascular endothelial cells exhibited counterclockwise torque, C2C12 myoblasts showed torque with slight clockwise bias. Moreover, an actin ring composed of transverse arcs and radial fibers was identified as a major factor determining the LR bias of cellular torque, since the disruption of actin ring by biochemical inhibitors or elongated cell shape abrogated the counterclockwise bias of NIH 3T3 fibroblasts. Our finding reveals a LR-biased torque of single cells and a fundamental origin of cytoskeletal chirality. More broadly, we anticipate that our method will provide a different perspective on mechanics-related cell physiology and force transmission necessary for LR propagation in tissue formation.**

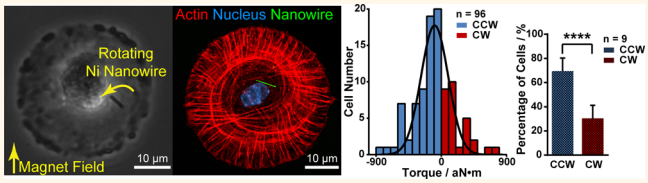

KEYWORDS: *left–right asymmetry, cell mechanics, nanowire, micropatterning, torque*

Mechanical forces between cells and microenvironment regulate many physiological functions.[1] For example, flow-mediated shear stress induces changes of endothelial cell morphology and differentiation.[2,3] Using micropatterning to control cell shape, remodeled cytoskeleton was also found correlated with apoptosis,[4] proliferation[5] and osteogenic differentiation.[6] Notably, such physical stimuli applied externally were found coupled with the force generated by cells.[7,8] Using arrays of elastomer microposts having different elastic moduli, reports showed that stiffer microposts can stimulate cells to exert greater contractile force,[8−10] which is positively correlated with the size of focal adhesion[9,10] and mediates the lineage commitment.[9,11] Clearly, since cell mechanics participates in many aspects of cell physiology, the ability to characterize cellular force is crucially important.

Recently, a variety of cell mechanics was reported with left–right (LR) asymmetry.[12,13] Evidence was found in embryonic development, such as blastomeres' uneven distribution[14] and epithelium rotation of hindgut tube,[15] and in culture, such as cell alignment,[16−18] migration,[17,19] and cell–cell assembly.[17] In particular, actomyosin activity was found essential for such LR asymmetric mechanics in both single cell level[16,17,20,21] and tissue/organ development.[12,14,22−26] Because actomyosin activity is also associated with cellular force,[9,10,27] it predicts a type of cellular force that mediates the LR-biased mechanics and eventually coordinates the formation of LR asymmetry in tissue architecture. However, the existing platforms to characterize cellular force, including traction microscopy,[28−31] magnetic attraction,[7,8] atomic force microscopy,[32] and arrays of elastomer microposts,[8−10] mainly focus on cell contractility. Due to the lack of appropriate platform, cellular force with LR bias has yet to be found.

Here we report a nanowire magnetoscope that reveals a rotating force—LR-biased torque—exerted by cells. Ferromagnetic nickel nanowires[33−37] were deposited into cell culture with a horizontal and uniform magnetic field externally applied (Figure 1a). After internalized by cells, the nanowires that originally aligned with the horizontal magnetic field were

Received: February 14, 2016
Accepted: July 7, 2016
Published: July 7, 2016

DOI: 10.1021/acsnano.6b01142
ACS Nano 2016, 10, 7409–7417

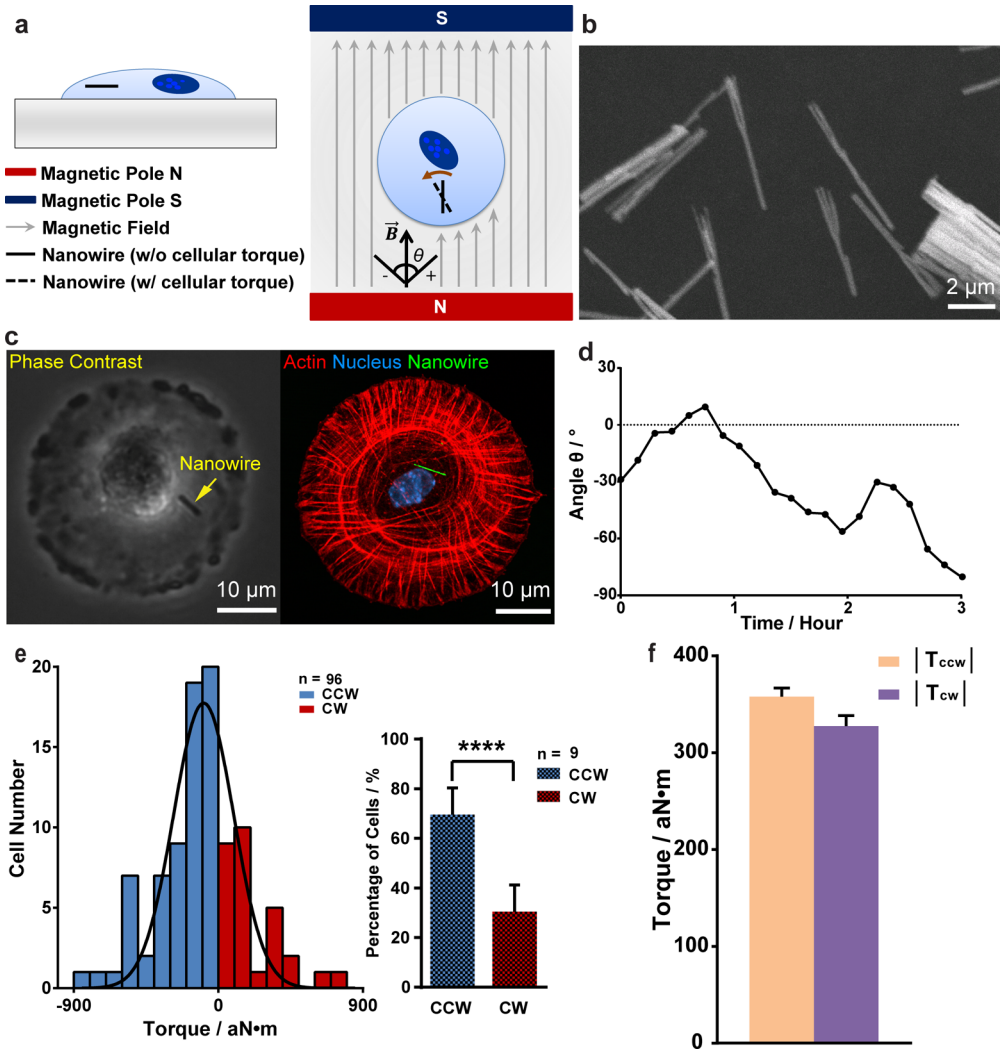

Figure 1. Working principle of the nanowire magnetoscope for characterizing cellular torque with LR bias. (a) The schematic of the nanowire magnetoscope. The ferromagnetic nanowires were deposited into cells cultured on circular cell-adherent islands. With a uniform, horizontal magnetic field applied externally, the ferromagnetic nanowires that first aligned with the magnetic field (solid) were subsequently internalized and rotated (dashed) due to the cellular torque. (b) The nickel nanowires imaged by scanning electron microscope. (c) Phase contrast and confocal microscopy of a single cell spreading on a circular pattern with a nanowire internalized. (d) Time-lapse microscopy tracing the nanowire rotation in a 3-h duration. (e) Histogram of the cellular torque of NIH 3T3 fibroblasts based on the average of torque measured at each snapshot within a single cell during the 3-h duration ($\vec{B}$ = 30 G, island area = 3000 μm^2). The percentages of cells with CW or CCW torque were obtained from repeated experiments and compared by student t test (mean ± SD, $P \leq 0.0001$). (f) The magnitude of torque of NIH 3T3 fibroblasts by averaging the absolute torque of all snapshots in CW direction, $|T_{cw}|$ (n = 757), or in CCW direction, $|T_{ccw}|$, (n = 1259) (mean ± SEM).

rotated owing to the torque generated by cells. This torque is LR-biased depending on cell types. While NIH 3T3 mouse fibroblasts and human vascular endothelial cells (hVECs) exhibited counterclockwise (CCW) torque, C2C12 mouse myoblasts showed a slight clockwise (CW)-biased torque. Moreover, using the quantitatively measured torque and the analysis of subcellular actin distribution, we found that an actin ring composed of transverse arcs and radial fibers determines the LR bias of the cellular torque. Together, our finding of LR-biased cellular torque measured by the nanowire magnetoscope offers an approach to reveal cell's rotational force and a fundamental framework to explain single cell's LR asymmetry. Moreover, as a different type of cellular force, it creates a possibility to investigate mechanics-mediated cell physiology and force transmission necessary for LR formation in tissue development.

RESULTS AND DISCUSSION

LR-Biased Cellular Torque Derived by Nanowire Magnetoscope. Cells were cultured on micropatterned cell-adherent islands with defined shapes to allow cells rotating at a fixed position. After cell settlement, ferromagnetic nanowires (Figure 1b) were deposited and spontaneously internalized by the cells (Figure 1c).[33−37] The internalization was validated using confocal microscopy (Figure S1), and cells remained viable (Figure S2). Notably, only single cells on cell-adherent islands with single nanowires were analyzed. With a pair of permanent magnet placed around the cell culture, a uniform, horizontal magnetic field was created, with which nanowires were first aligned (Figure 1a). Subsequently, the cells exerted a torque against the magnetic alignment force, causing the nanowires to orient with an angle CW or CCW deviating from

DOI: 10.1021/acsnano.6b01142
ACS Nano 2016, 10, 7409−7417

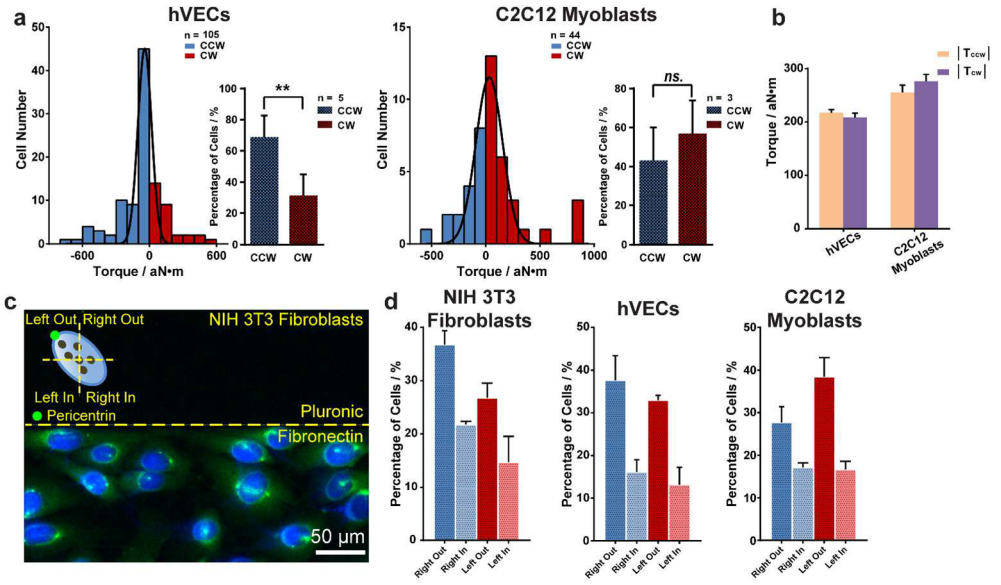

Figure 2. LR-based cellular torque and polarity depending on cell types. (a) Histogram of the cellular torque of human vascular endothelial cells (hVECs), and C2C12 myoblasts ($\vec{B}$ = 30 G, island area = 3000 μm^2), and the percentages of cells with CW or CCW bias (mean ± SD, $P \leq 0.01$ for hVECs). (b) The magnitude of torque of hVECs and C2C12 myoblasts in CW direction, $|T_{cw}|$ (n = 782, 567), or in CCW direction, $|T_{ccw}|$ (n = 1423, 357) (mean ± SEM). (c) When cultured on alternating stripes of cell-adherent (fibronectin) and cell-repellent (pluronic) substrates, for cells adjacent to the stripe boundary, the cell polarity was classified by the location of pericentrin (green) in quadrants of Right Out, Right In, Left Out, and Left In relative to the nucleus (blue). The horizontal axis refers to the orientation of the substrate boundary. (d) The distribution of cell polarity (triplicated experiments; total number of cells = 1137, 1504, and 1867 for NIH 3T3 fibroblasts, hVECs, and C2C12 cells, respectively).

the magnetic field (Figure 1a), allowing a quantitative measurement of cellular torque.

We first tested whether cells were enabled to rotate with LR bias in this setting. Nuclei of live NIH 3T3 fibroblasts were stained with fluorescence to observe their rotational movement (Figure S3a). The result showed that NIH 3T3 fibroblasts had a slight CCW bias in their angular velocity (Figure S3b). Interestingly, after nanowire internalization, the nucleus rotation became slower and significantly biased in CCW direction (Figure S3b,c), suggesting that the chirality was provoked. Importantly, when cultured in the magnetic field ($\vec{B}$ = 30G) with a single nanowire internalized, the angular velocity of nucleus remained CCW-biased (Figure S3b,c), suggesting that the LR bias was unaffected by the applied magnetic field.

The nanowire magnetoscope was used to continuously track the nanowire rotation and the associated torque (Figure 1d and Movie S1). The rotational angle, θ, is defined positive for CW and negative for CCW rotation (Figure 1a). Because the moment of inertia of nanowires is negligible, the rotational angle of each snapshot can be considered as the quasi-steady-state, where the magnetic moment and the cellular torque can be considered as in equilibrium. As such, the cellular torque was measured according to $\vec{\tau} = \vec{\mu} \times \vec{B} = |\vec{\mu}| \cdot |\vec{B}| \cdot \sin\theta$, where $\vec{\tau}$ is the magnetic torque, $\vec{\mu}$ is the magnetic moment of the nanowire, $\vec{B}$ is the external magnetic field, and θ is the rotational angle of the nanowire. Magnetic moment was estimated using the saturation moment scaled with the nanowire length: $|\vec{\mu}|/L = 3.9 \times 10^{-14}$ N·m/μm·T.[35,36] Thus, after collecting the torque measured at each snapshot of each single cell (example in Figure S4), the LR bias of each cell can be seen by an average torque of different time points within that single cell (Figure 1e), and the overall magnitude can be quantified by the absolute torque of all snapshots in CCW direction, $|T_{ccw}|$, or CW direction, $|T_{cw}|$ (Figure 1f). We found that NIH 3T3 fibroblasts cultured on circular islands ($\vec{B}$ = 30 G, island area = 3000 μm^2) exhibited a CCW-biased torque (Figure 1e). This LR bias increased over time, and appeared to be significant after cultured for 2−3 h (Figure S5). The magnitude of the cellular torque fell in the range of 300−350 aN·m for NIH 3T3 fibroblasts, in which $|T_{ccw}|$ is slightly higher than $|T_{cw}|$ (Figure 1f). Notably, the cellular torque seems to be independent of the nanowire location, though most nanowires intended to locate near the centroid of cells (<60% of cell radius, Figure S6), suggesting that the measured cellular torque is an overall behavior when considering a single cell as a rotational unit.

LR-Biased Cellular Torque Is Cell-Type Dependent and Associated with Other Types of LR Asymmetry. In fact, the nanowire magnetoscope is a universal platform for other adherent cells. Two more cell types, C2C12 mouse myoblasts and hVECs, were tested. The results showed that hVECs exhibited a CCW-biased torque, while C2C12 myoblasts showed a slight CW-biased torque, although it is less statistically significant (Figure 2a,b). This cell-type dependence was also reported in other types of LR asymmetries, *i.e.*, cell orientation[16] and polarity,[17] suggesting a possibility that other types of LR-biased cell behavior may be closely associated with this LR-biased torque. To validate it, we studied the cell LR polarity and orientation for comparison. In brief, cells were plated on alternating stripes of cell-adherent (fibronectin) and cell-repellent (pluronic) substrates. Previously we have learned that cells near the stripe boundary would accumulate their stress fibers, which were found essential to activate the LR bias in cell polarity.[16,17] The cell polarity was defined by the location of pericentrin relative to the nucleus centroid, and classified as Right Out, Right In, Left Out, and Left In of cells adjacent to the substrate boundary (Figure 2c). The result showed that NIH 3T3 fibroblasts, which exhibited CCW-biased torque, had a rightward bias in their polarity

DOI: 10.1021/acsnano.6b01142
ACS Nano 2016, 10, 7409−7417

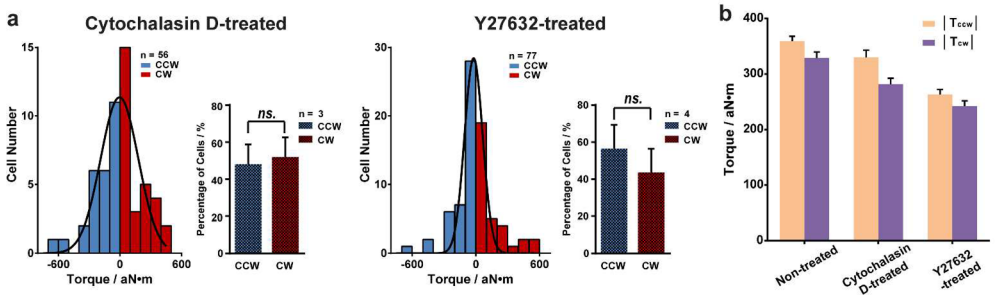

Figure 3. LR bias of cellular torque abolished by actin inhibitor. (a) Histogram of the cellular torque of NIH 3T3 fibroblasts treated with actin inhibitor cytochalasin D or Y27632 ($\vec{B}$ = 30 G, island area = 3000 μm^2), and the percentages of cells with CW or CCW bias (mean ± SD). (b) The magnitude of torque of nontreated, cytochalasin D-treated, or Y27632-treated NIH 3T3 fibroblasts in CW direction, $|T_{cw}|$ (n = 757, 634, 823), or in CCW direction, $|T_{ccw}|$ (n = 1259, 542, 794) (mean ± SEM).

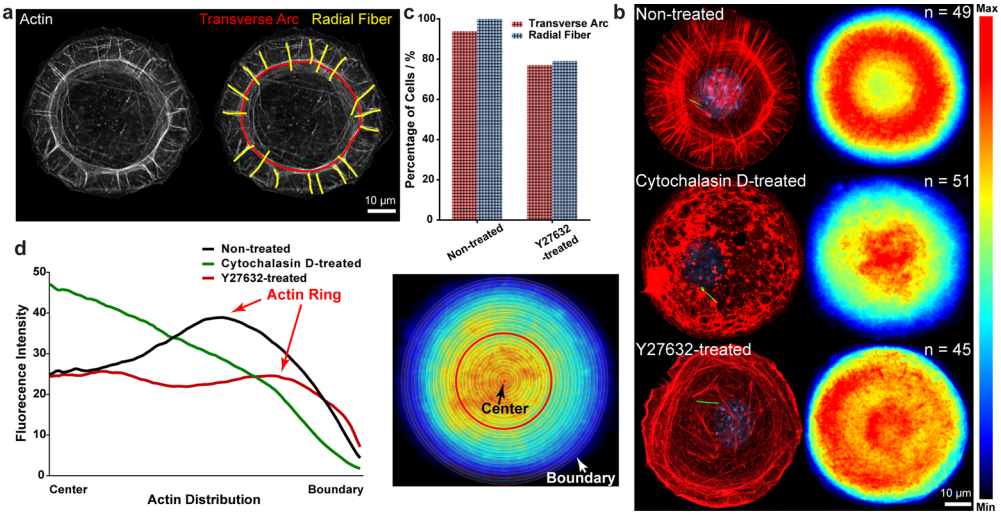

Figure 4. An actin ring underlying the LR bias of cellular torque. (a) Confocal microscopy image of actin filaments (white) of a cell on a circular pattern showing a ring structure composed of transverse arcs (red) and radial fibers (yellow). (b) Confocal microscopy images of the actin filaments of nontreated, cytochalasin D-treated or Y27632-treated NIH 3T3 fibroblasts (left) and the heat map of actin distribution after image stacking (right). (c) The percentage of nontreated (n = 50) and Y27632-treated (n = 50) NIH 3T3 fibroblasts showing transverse arcs or radial fibers. (d) Curves of actin distribution with respect to the radial axis of nontreated, cytochalasin D-treated or Y27632-treated NIH 3T3 fibroblasts. By dividing the heat maps into 100 concentric ring regions (right), the mean fluorescence intensity of each ring region was plotted with respect to its radius (left).

(Figure 2d). Consistently, the CCW bias of hVECs and CW bias of C2C12 myoblasts also led to a rightward and leftward polarity, respectively (Figure 2d). Moreover, by studying the cell orientation with respect to the horizontally aligned stripe boundary, consistently, we also found a rightward bias in NIH 3T3 fibroblasts and hVECs and a leftward bias in C2C12 myoblasts (Figure S7). Importantly, our result agrees with the literatures that NIH 3T3 and hVECs has the same LR-biased direction other than that of C2C12 myoblasts.[16] Together, it suggests that the LR-biased cellular torque is cell-type dependent and associated with other types of LR asymmetry.

Actin Ring Plays an Important Role in Regulating the LR-Biased Cellular Torque. The nanowire magnetoscope can be easily integrated with conventional assays for more comprehensive characterization, as this system allows biochemical treatments on cells and monitoring them under a microscope. As a demonstration, we integrated it with pharmacological inhibitors to elucidate the role of actin, which is closely related to cell contractility,[27,38] and likely related to the LR bias of cellular torque. NIH 3T3 fibroblasts on optimized settings ($\vec{B}$ = 30 G, island area = 3000 μm^2) were used for this study because they exhibited the greatest magnitude and LR bias of torque (Figure 1f, Figure 2b and Figure S8). Two kinds of actin inhibitors, Y27632 that inhibits the upstream Rho-associated kinase (ROCK) and cytochalasin D that prevents actin polymerization, were used. Remarkably, the LR bias was suppressed when treated with Y27632 and neutralized when treated with cytochalasin D (Figure 3a). The magnitude of torque, $|T_{cw}|$ or $|T_{ccw}|$, decreased after either treatment, although $|T_{ccw}|$ was still greater than $|T_{cw}|$ (Figure 3b). Thus, the treatment of actin inhibitors abolished the LR bias and suppressed the magnitude of cellular torque.

Fluorescence labeling and image stacking with registration can be further integrated with the nanowire magnetoscope to create a heat map distribution of intracellular components, *e.g.*, actin, and investigate their roles. The results showed that there exists a ring structure composed of two classes of actin filaments: radial fibers and transverse arcs.[39,40] Transverse arcs are curved actin filaments in parallel with cell periphery, while radial fibers are actin filaments that intersect with transverse arcs and point toward the periphery (Figure 4a). After image stacking, there was a clear actin ring around the cell periphery, suggesting the dominance of transverse arcs and radial fibers (Figure 4b). However, such ring structure and actin filaments

DOI: 10.1021/acsnano.6b01142
ACS Nano 2016, 10, 7409–7417

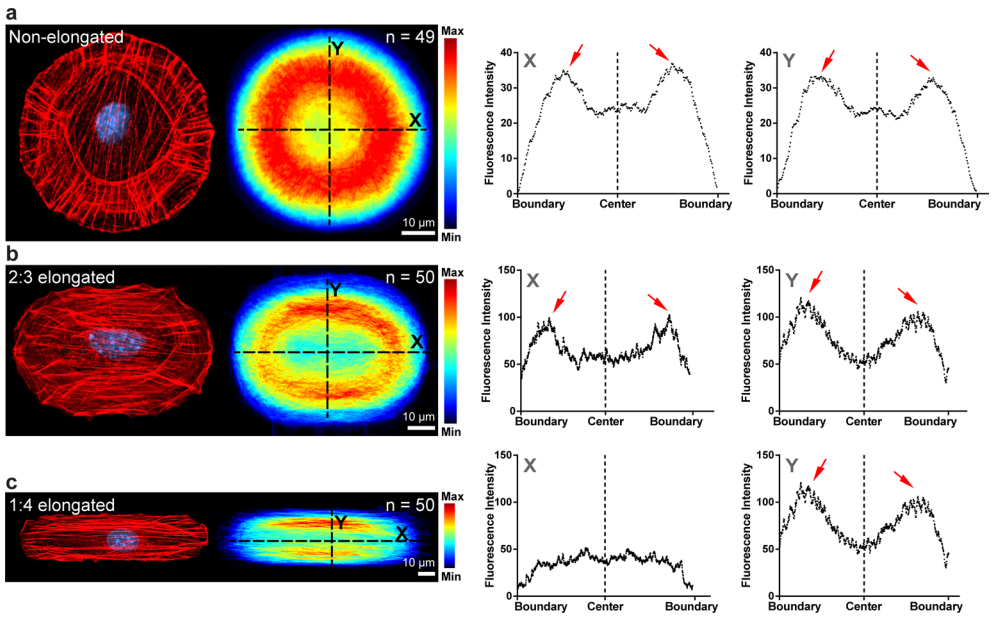

Figure 5. Actin ring of cells spreading on islands with different aspect ratio (AR). Confocal microscopy images of actin filaments of NIH 3T3 fibroblasts (left), the heat map of actin distribution after image stacking (middle), and its actin distribution along *x*- or *y*-axis across the centroid (right) of cells on (a) nonelongated, circular islands, (b) partially elongated islands (AR = 2:3) and (c) fully elongated islands (AR = 1:4).

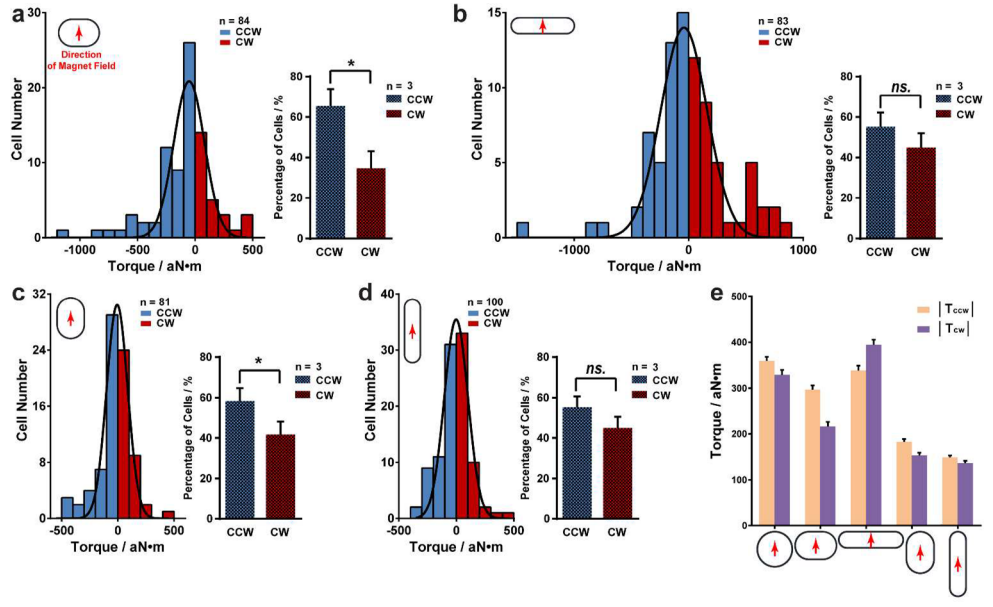

Figure 6. LR-biased cellular torque of cells spreading on elongated islands. (a–d) Histogram of the cellular torque of NIH 3T3 fibroblasts on elongated cell-adherent islands with aspect ratio (AR) at 2:3 (a, c) or 1:4 (b, d), and the percentages of cells with CW or CCW bias (mean ± SD, $P \leq 0.05$ for AR = 2:3). The long axis was placed either perpendicular (a, b) or parallel (c, d) to the magnetic field $\vec{B}$. (e) The magnitude of torque of circular, 2:3 elongated (perpendicular to $\vec{B}$), 1:4 elongated (perpendicular to $\vec{B}$), 2:3 elongated (parallel to $\vec{B}$), 1:4 elongated (parallel to $\vec{B}$) NIH 3T3 fibroblasts in CW direction, $|T_{cw}|$ (n = 757, 648, 796, 778, 992), or in CCW direction, $|T_{ccw}|$ (n = 1259, 1016, 947, 923, 1108) (mean ± SEM).

were fully dissembled in cells treated with cytochalasin D (Figure 4b). For Y27632-treated cells, the actin ring was also significantly suppressed (Figure 4b), and the percentages of cells having either transverse arcs or radial fibers were both decreased (Figure 4c). Moreover, by dividing the heat maps into 100 concentric ring regions, the average intensity in each ring region with respect to its radius showed a distinct peak representing the actin ring in nontreated cells. This peak was reduced in Y27632-treated cells and disappeared in cytochalasin D-treated cells (Figure 4d). Consequently, since LR bias and actin ring were both abolished after treating the inhibitors, the actin ring may determine the LR bias of cellular torque.

Additionally, by altering the shape of cell-adherent islands, the role of actin ring can be further elucidated. While maintaining the area constant, the circular shape was partially or fully elongated into ellipse with aspect ratio (AR) at 2:3 or 1:4, respectively. Comparing to cells on circular islands that have actin forming a ring shape (Figure 5a), the actin ring was

DOI: 10.1021/acsnano.6b01142
ACS Nano 2016, 10, 7409–7417

thinner but still observable on partially elongated islands (AR = 2:3) (Figure 5b). In contrast, on fully elongated island (AR = 1:4), the actin ring discontinued at the short edge such that the ring structure was broken into two clusters of linear fibers aligning along the long edges (Figure 5c). To further highlight the difference, we plotted the actin distribution along the *x*- and *y*-axis across the centroid of cells (Figure 5a–c). We can clearly see that for cells on circular and 2:3-elongated islands, there were dual peaks of actin distribution along the *x*- and *y*-axis, indicating that the actin ring continuously appeared along the circumference. However, for cells on 1:4-elongated islands, while the dual peaks were still observed in actin distribution along the *y*-axis, the peaks disappeared along the *x*-axis, indicating that the actin ring was broken and discontinued.

We next applied the nanowire magnetoscope to study the cellular torque on elongated islands. We found that the LR bias was less significant in cells on partially elongated islands (AR = 2:3) and neutralized on fully elongated islands (AR = 1:4) (Figure 6a–d). This change of LR bias was consistently observed when the long axis of elongate cells was perpendicular (Figure 6a,b) or parallel (Figure 6c,d) to $\vec{B}$. Thus, it validates that the actin ring is required for the LR bias. Moreover, for partially elongated cells (AR = 2:3), the magnitude of torque was reduced regardless the orientation of long axis (Figure 6e). This suppression of torque magnitude may be due to the thinner actin ring in partially elongated cells (Figure 5b). In contrast, for fully elongated cells (AR = 1:4), the magnitude of torque increased when the long axis was perpendicular to $\vec{B}$ but reduced when the long axis was parallel to $\vec{B}$. We reason that the fully elongated shape and the presence of linear fibers may make the nanowires preferably aligning with the long axis, therefore constraining the nanowire rotation and affecting the torque exhibition. Altogether, these findings conclude that the actin ring is necessary for revealing the LR bias in cellular torque. This result may further explain why the cellular torque cannot be observed with consistent and definite LR bias in conventional culture wells (Figure S9), in which the unbounded cell shape changes dynamically such that the actin ring cannot be consistently organized, veiling the intrinsic LR bias.

Discussion. In this paper, we developed a nanowire-based platform that can quantitatively measure the cellular torque with LR bias. Although the expression of chirality is essential for this measurement, how it is induced by nanowire internalization is not fully understood (Figure S3). Recent research indicates that nanoparticles may generate reactive oxygen species that affect cell behaviors such as viability.[33,41] More importantly, internalization of nanoparticles is also related to LR asymmetry of cells. When cells were cultured on ring-shape substrate, internalization of carbon nanotubes mediated oxidative stress which thickened and rearranged the actin filaments toward cell periphery, eventually leading to the loss of chiral migration.[18] In our experiment, we also found that the actin filaments were intensified after nanowire internalization. Comparing cells with nanowires to cells without nanowires, although the spatial distribution of actin filaments remained similar (Figure 4b and Figure S10a), the fluorescence intensity of actin in cells indeed increased after nanowire internalization (Figure S10b). This increase was observed even with the treatment of actin inhibitor cytochalasin D or Y27632. This result is consistent with our previous findings that the cellular LR asymmetry was induced in response to the accumulation of actin stress fibers when cells were migrating across a substrate interface.[17] Hence, we speculate that this enhanced chiral movement upon nanowire internalization is because of the increased assembly of actin filaments essential for the exhibition of LR bias.

Using the quantitatively measured torque and the analysis of subcellular actin distribution, we found that an actin ring composed of transverse arcs and radial fibers is the key factor determining the LR bias of the cellular torque. By comparing the results of two different approaches that disrupt different aspects of actin ring, *i.e.*, disassembly of actin filaments by actin inhibitor or discontinuity of actin ring by cell shape change, the LR bias was all abolished. These results collectively suggest that the actin ring is essential for the exhibition of LR bias in cellular torque. This finding is also consistent with the literature,[20] in which radial fibers were unidirectional tilted accompanying with a tangential shift in the retrograde movement of transverse arcs and centripetally growing radial fibers. Thus, the LR bias of cellular torque could be a result of the rotational movement of actin ring that generates a CW or CCW offset. In addition, since the rate of actin's retrograde flow should be similar in one cell type, this may explain the reason why the magnitude of $|T_{cw}|$ and $|T_{ccw}|$ was similar, even though the percentage of CW- or CCW-biased cells were significantly different.

Notably, our result indicated that this LR-biased torque is cell-type dependent and associated with other LR asymmetry. It suggested that the rotational movement of transverse arcs may be also biased in CW or CCW direction depending on cell types. Such rotational movement can be considered as the tangential shift along the boundary of circular pattern. Thus, when cultured on cell-adherent stripes, we speculate that the assembling process of stress fibers may involve the tangential shift of transverse arcs along the stripe boundary, which subsequently drives a lateral shift of intracellular apparatus and causes the LR-biased cell polarity. Ultimately, *via* a series of cell–cell interaction and LR-biased migration, the LR-biased cell polarity then leads to the cell orientation with specific LR as described previously.[42]

Furthermore, we also found that, for cells on conventional culture wells (Figure S9), the LR bias was insignificant. Referring to the result from cells on circular or elongated islands, it is clear that the actin ring in circular cells is essential for the exhibition of LR bias. This may potentially explain the inconsistent LR bias observed from cells cultured without boundary constraint, in which cell shape changes dynamically such that the actin ring cannot be consistently organized. Thus, the cell movement, which combined both the LR-biased motion by actin ring and the nonbiased motion by linear stress fibers, should therefore be indefinite and inconsistent in their LR bias, even if the nanowire is internalized.

To investigate the potential correlation between the chiral alignment of radial fibers and the cellular torque, NIH 3T3 fibroblasts on circular islands ($\vec{B}$ = 30 G, island area = 3000 μm^2) were fixed at the end of 3-h duration for analysis. Our result showed that only 22.38% of cells exhibited the chiral orientation of radial fibers, which is consistent with the findings that chiral swirling stage of actin fibers only occurs for several hours within the 12 h of recorded period.[20] For the cells with chiral orientation, 66% of them were CCW-biased, which is consistent with the CCW-biased torque of NIH 3T3 fibroblasts (Figure S11a). Interesting, however, the direction of actin chirality does not fully match the generated cellular torque at that snapshot (Figure S11b). Since both cellular torque and actin chirality are dynamically changing in every sec, this

DOI: 10.1021/acsnano.6b01142
ACS Nano 2016, 10, 7409–7417

mismatch may be due to the phase difference between the generation of cellular torque and the tilted orientation of radial fibers.

CONCLUSION

Mechanical force is pervasive in regulating cell physiology and morphogenesis. The dependence of LR asymmetry on actomyosin activity suggests an existence of cellular force with LR bias, but it is yet to be found. In this paper, we report a nanowire magnetoscope that reveals a LR-biased cellular torque based on internalized nanowires rotating within a uniform and horizontal magnetic field. Importantly, this torque is LR-biased depending on cell types, and associated with other types of LR asymmetry such as cell LR polarity and orientation. Moreover, using the quantitatively measured torque and the analysis of subcellular actin distribution, we found that an actin ring composed of transverse arcs and radial fibers is the key factor determining the LR bias of cellular torque. To our knowledge, it is a first demonstration of LR-biased torque generated by cells, which is clearly independent of other biophysical characteristics such as the widely studied cell contractility. As cell mechanics regulates many physiological behaviors, cellular torque may also play a role and opens up possibilities for mechanobiology and stem cell research. In addition, the identification of actin ring as the key factor in the LR bias of cellular torque reveals the origin of cytoskeletal chirality and provides a mechanistic insight of cytoskeletal structure. Furthermore, the existence of such torque indicates that there may be mechanical interactions of cells between their neighboring cells or substrates necessary to unfold the cellular torque to the LR asymmetry in tissue architecture. The nanowire magnetoscope, as a universal platform applicable to most cell types, can therefore be applied to trace the cellular torque, enabling the study of the regulatory mechanism in the developmental process and tissue regeneration in the future.

METHODS

Cell Culture and Treatment. Three cell types, NIH 3T3 mouse fibroblasts, C2C12 mouse myoblasts, and hVECs were used. For NIH 3T3 fibroblasts, the growth medium is Dulbecco's Modified Eagle Medium/Nutrient Mixture F-12 (DMEM/F-12) supplemented with 10% fetal bovine serum (FBS) and 1% penicillin-streptomycin (PS). For C2C12 myoblasts, the medium is DMEM (4 mM L-glutamine, 4500 mg/L glucose, 1 mM sodium pyruvate, and 1.5 g/L sodium bicarbonate) supplemented with 10% FBS and 1% PS. The hVECs were cultured in Endothelial Cell Growth Medium (Lonza). For treatments of actin inhibition, 1 μM of cytochalasin D (Thermo Fisher) or 10 μM Y27632 (Alexis) were applied to the cell culture.

Nanowire Synthesis, Separation and Characterization. Ferromagnetic nickel nanowires were synthesized by electrochemical deposition. We used a two-electrode electrochemical system. A nickel wire with 1.0 mm diameter (Alfa Aesar) was used as counter electrode. Alumina filter membrane with 100 nm pores was used as the template (Whatman). With Ga–In alloy (Sigma) coated on one side, the membrane can be electro-conductive to a copper sheet, which serves as the working electrode. Nickel was electroplated into those pores in electrolyte containing 20 g/L nickel(II) chloride hexahydrate, 515 g/L nickel(II) sulfamate tetrahydrate, and 20 g/L boric acid. The voltage was supplied and controlled by a DC power supply (GW Instek). The whole reaction was carried out at room temperature without stirring or other special treatment. After 15 min deposition under 15v DC voltage, we can yield the nanowires with the length of 8.87 ± 1.53 μm and diameter of 280 ± 63 nm (mean ± SD), as measured by scanning electron microscope (JSM-5600, JEOL). Next, concentrated nitric acid was used to remove the Ga–In alloy film, followed by dissolving the template in 70 °C KOH bath (pH = 12.8) overnight with ultrasonication applied occasionally. At last, the nanowires were sterilized and stored in absolute ethanol. To resuspend and separate nanowires, the nanowires were first immersed in 1% Tween-20 solution and vortex for 30 min. After rinsing with 0.5% Tween-20 for three times, the nanowires were resuspended in 0.05% Tween-20 solution. Before applying to cell culture, the nanowires were rinsed with fresh culture media for three times with occasional ultrasonication to ensure that the solution was fully refreshed. For each transfer procedure, we used a permanent magnet to collect the nanowires, followed by removing the supernatant and replenishing with fresh solution. Transmission electron microscopy (JEM-2100F, JEOL) and energy-dispersive X-ray spectroscopy (X-MAN^N, Oxford Instrument) showed that the nanowires are single crystalline without oxidation, and the lattice space is 0.26 nm, which is comparable to (111) plane's interplanar distance of Ni structure (Figure S12) and consistent with previous literatures that used electrochemical deposition in alumina filter membrane.[43−45]

Micropatterning. Photolithography was used to control cell shape and spreading. Fibronectin, one of extracellular protein for cell attachment,[46] was used for cell-adherent islands, while pluronic, a nonionic copolymer surfactant, which can bind with hydrophobic surface therefore block the protein adsorption and cell adhesion,[47] was used for cell-repellent regions. Glass slides were cleaned by acidic bath (H_2SO_4:H_2O_2 = 3:1) at 100 °C for 20–40 min, followed by rinsing with DI water and drying by compressed air flow. After dehydration baking using a silicon wafer hot plate (SawaTec) at 120 °C for 5 min, the slides were coated with hexamethyldisilazane (HMDS, Sigma) for 8 min at room temperature. Positive photoresist AZ 5214 (AZ Electronic Materials) was spin-coated on the slides by 3000 rpm for 30 s with 1000 ramping to form a ∼1 μm thin layer, and then soft baked at 100 °C for 2 min. After exposed under UV light (5 mW/cm^2) for 120 s through a photomask aligner (Optical Associates), the photoresist pattern was developed using the developer (AZ400K:DI water = 1:2) for 10 s for each chip to remove the exposed AZ 5214 photoresist. A 2 min plasma treatment (air plasma, 200 W, 500 mTorr, Harrick Plasma) was followed to remove the residual photoresist and HMDS in the exposed regions. Next, the slides were coated with HMDS again for 8 min. Fifty μg/mL fibronectin solution (Thermos Fisher) was then used to coat on the chip for 30 min as fibronectin can be adsorbed on HMDS substrate and form the cell-adherent islands. Afterward, the undeveloped photoresist was removed by absolute ethanol with sufficiently rinsing and ultrasonication (80W, 5 s per pulse). Finally, the slides were dried with compressed air flow and stored in 4 °C refrigerator. Immediately before plating cells, 1% pluronic (Sigma) was coated on the chip for 30 min to form the cell-repellent region.

Nanowire Magnetoscope for Measurement of Cellular Torque. Cell-adherent islands were designed as circles with areas of 2000–5000 μm^2. The circular patterns were also elongated as ellipse such that the aspect ratio was changed to 1:4 or 2:3. The cells were seeded on the chip with the same number of patterns to facilitate single cells on single patterns. For experiments on conventional culture wells, cells were plated at a density of 1600 cells per cm^2. After 3 h for cell settlement, cells were either nontreated or treated with cytochalasin D or Y27632 for 1 h. Next, the cell culture dish was placed in Chamlide TC incubator system (Live Cell Instrument) perfused with 5% CO_2 at 37 °C. A pair of permanent magnet was placed around the culture dish to create a uniform and horizontal magnetic field with $\vec{B}$ = 30 G, 21 G or 11.5G. Nickel nanowires were then deposited into cell culture at wires to cell ratio at 10:1. Forty min after nanowire deposition, the nanowires' rotation was monitored and captured using Nikon Eclipse Ti-E microscope. Only single cells fully spreading on cell-adherent islands with single nanowires internalized were selected for analysis. We analyzed the rotational angles of nanowires in three cell types in regular culture condition or treated with cytochalasin D or Y27632. Using the time-lapse microscopy, the rotational angles of nanowires, which were used to derive the cellular torque, were recorded at every 9 min, To elucidate the LR bias, the torque representing each single cell was calculated based on the

DOI: 10.1021/acsnano.6b01142
ACS Nano 2016, 10, 7409–7417

averaged torque measured within the single cell during the entire time course. We analyzed the percentage of cells with CCW and CW bias based on multiple independent experiments that involve different number of cells. The percentages of cells with CCW or CW bias were obtained in each experiment, and the value was averaged across different experiment (mean ± SD). The difference between CCW and CW bias was then analyzed by student t test to evaluate the statistical significance of LR bias. For the magnitude, we used the absolute torque at either direction (CW or CCW) of each snapshot of all cells to calculate the $|T_{cw}|$ and $|T_{ccw}|$.

Cell Viability. NIH 3T3 fibroblasts were cultured on 3000 μm^2 circular pattern. Ten min after nanowire deposition, the cells were incubated with 1 μM DEVD-NucView488 (Biotium) and imaged within 0.5−6 h. Among the population of single cells with single nanowires, the cell viability was obtained based on the percentage of cells without fluorescence staining in the nucleus.

Cell Polarity. For the cell polarity assay, micropatterned cell-adherent stripes with 300 μm width were used, where cells were seeded at the density of 50000 cells per 2 × 2 cm^2 and cultured in 5% CO_2 at 37 °C humidified incubator for 12 h. Afterward, cells were fixed by −30 °C methanol for 15 min and blocked by Image-iT FX signal enhancer (Thermo Fisher) for 30 min. Next, the rabbit antipericentrin (1:500, Covance) was applied for 1 h at room temperature, followed by goat antirabbit antibody (1:1000, Thermo Fisher) for 30 min and DAPI (300 nM, Thermo Fisher) staining for 10 min. At last, the samples were mounted by Fluoromount-G Slide Mounting Medium (Electron Microscopy Sciences), and the fluorescence images were taken by the inverted fluorescence microscope (Nikon). By orienting the stripe boundary horizontally, the polarity was determined by the location of pericentrin in quadrants of Right Out, Right In, Left Out, and Left In relative to nucleus for cells adjacent to the stripe boundary.

Cell Orientation. Cell orientation assay were performed on micropatterned cell-adherent stripes with 300 μm width. NIH 3T3 fibroblasts, human vascular endothelial cells (hVECs), or C2C12 myoblasts were seeded at the final density of 93895 cells, 44000 cells and 58200 cells per cm^2 respectively and cultured in 5% CO_2 at 37 °C humidified incubator for 12 h. Afterward, cells were fixed by 4% paraformaldehyde for 15 min at 4 °C and stained with DAPI (300 nM, Thermo Fisher) for 10 min. At last, the samples were mounted by Fluoromount-G Slide Mounting Medium (Electron Microscopy Sciences), and the fluorescence images were acquired by the inverted fluorescence microscope (Nikon). By placing the stripes horizontally, the cell orientation was determined by the angle of nucleus's long axis relative to the stripe boundary as either rightward (+) or leftward (−), φ. The orientation angle was analyzed by the regionprops function of MATLAB.

Live Nucleus Rotation Analysis. NIH 3T3 fibroblasts were cultured on 3000 μm^2 circular pattern and incubated with 10 μg/mL bisBenzimide H 33342 trihydrochloride (Sigma) for 30 min to obtain the fluorescence staining of nucleus. Cells were cultured in Chamlide TC incubator system perfused with 5% CO_2 at 37 °C and imaged using Nikon Eclipse Ti-E microscope at every 9 min for 3 h. The angular orientation of the nucleus' long axis was analyzed by the regionprops function of MATLAB. To characterize the cell rotation, the transient angular velocity of the nucleus' long-axis was calculated using the formula:

$$V_{mean} = \frac{\sum_{(n=2)}^{21} \left(\frac{\gamma(t_n) - \gamma(t_{n-1})}{t_n - t_{n-1}} \right)}{n-1} ^\circ/\text{min}$$

To elucidate the LR bias, the angular velocity representing each single cell was calculated based on the averaged transient velocity measured within a single cell during the entire time course. We analyzed the percentage of cells with CCW and CW bias based on multiple independent experiments that involve different number of cells. The percentages of cells with CCW or CW bias were obtained in each experiment, and the value was then averaged across different experiment (mean ± SD). The difference between CCW and CW bias was then analyzed by student t test to evaluate the statistical significance of LR bias. For the magnitude of velocity, we used the absolute value of transient velocity at each snapshot of all cells to calculate.

Fluorescence Labeling of Actin Filaments. NIH 3T3 fibroblasts were seeded on 3000 μm^2 circular pattern or elongated patterns with the aspect ratio as 1:4, or 2:3. After 3 h for cell settlement, cells were either nontreated or treated with cytochalasin D or Y27632 for 1 h, followed by incubation with or without nanowire for 40 min. Afterward, cells were fixed by 4% paraformaldehyde for 15 min at 4 °C and permeabilized using 0.2% Triton X-100 for 10 min. Image-iT FX signal enhancer was subsequently applied for 30 min. The actin filaments was labeled by rhodamine phalloidin (1:40, Thermo Fisher) for 1 h, followed by staining with DAPI (300 nM, Thermo Fisher) for 10 min and mounted by Fluoromount-G Slide Mounting Medium (Electron Microscopy Sciences). The images were captured by a confocal microscope (Leica) or an inverted fluorescence microscope (Nikon). As nickel nanowire is light-tight, their image can be captured by the reflected light with the excitation wavelength. To analyze the distribution of actin filaments, ∼50 images for each case were taken and stacked in MATLAB. Using the Regionprops functions, the cells were isolated from the background, and then the centroids of each cell were used as the registration marker, followed by normalization according to cell number to obtain an average grayscale image showing the distribution of actin filaments.

ASSOCIATED CONTENT

Supporting Information

The Supporting Information is available free of charge on the ACS Publications website at DOI: 10.1021/acsnano.6b01142.

Figures S1−S12 (PDF)

Movie S1 (AVI)

AUTHOR INFORMATION

Corresponding Author

*E-mail: thchen@cityu.edu.hk.

Notes

The authors declare no competing financial interest.

ACKNOWLEDGMENTS

We are pleased to acknowledge support from the National Natural Science Foundation of China (Grant No. 51305375), Idea Incubator Scheme (Grant No. 6987032) from City University of Hong Kong, and Early Career Scheme of Hong Kong Research Grant Council (Grant No. 21214815).

REFERENCES

(1) Wang, Y.; Wang, G. X.; Luo, X. D.; Qiu, J. H.; Tang, C. J. Substrate Stiffness Regulates the Proliferation, Migration, and Differentiation of Epidermal Cells. *Burns* **2012**, *38*, 414−420.

(2) Lam, R. H. W.; Sun, Y. B.; Chen, W. Q.; Fu, J. P. Elastomeric Microposts Integrated into Microfluidics for Flow-Mediated Endothelial Mechanotransduction Analysis. *Lab Chip* **2012**, *12*, 1865−1873.

(3) Obi, S.; Masuda, H.; Shizuno, T.; Sato, A.; Yamamoto, K.; Ando, J.; Abe, Y.; Asahara, T. Fluid Shear Stress Induces Differentiation of Circulating Phenotype Endothelial Progenitor Cells. *Am. J. Physiol. Cell Physiol.* **2012**, *303*, C595−C606.

(4) Chen, C. S.; Mrksich, M.; Huang, S.; Whitesides, G. M.; Ingber, D. E. Geometric Control of Cell Life and Death. *Science* **1997**, *276*, 1425−1428.

(5) Nelson, C. M.; Jean, R. P.; Tan, J. L.; Liu, W. F.; Sniadecki, N. J.; Spector, A. A.; Chen, C. S. Emergent Patterns of Growth Controlled by Multicellular Form and Mechanics. *Proc. Natl. Acad. Sci. U. S. A.* **2005**, *102*, 11594−11599.

(6) Kilian, K. A.; Bugarija, B.; Lahn, B. T.; Mrksich, M. Geometric Cues for Directing the Differentiation of Mesenchymal Stem Cells. *Proc. Natl. Acad. Sci. U. S. A.* **2010**, *107*, 4872−4877.

DOI: 10.1021/acsnano.6b01142
ACS Nano 2016, 10, 7409−7417

(7) Wang, N.; Butler, J. P.; Ingber, D. E. Mechanotransduction Across the Cell Surface and Through the Cytoskeleton. *Science* **1993**, *260*, 1124−1127.
(8) Sniadecki, N. J.; Anguelouch, A.; Yang, M. T.; Lamb, C. M.; Liu, Z.; Kirschner, S. B.; Liu, Y.; Reich, D. H.; Chen, C. S. Magnetic Microposts as an Approach to Apply Forces to Living Cells. *Proc. Natl. Acad. Sci. U. S. A.* **2007**, *104*, 14553−14558.
(9) Fu, J. P.; Wang, Y. K.; Yang, M. T.; Desai, R. A.; Yu, X. A.; Liu, Z. J.; Chen, C. S. Mechanical Regulation of Cell Function with Geometrically Modulated Elastomeric Substrates. *Nat. Methods* **2010**, *7*, 733−736.
(10) Tan, J. L.; Tien, J.; Pirone, D. M.; Gray, D. S.; Bhadriraju, K.; Chen, C. S. Cells Lying on a Bed of Microneedles: An Approach to Isolate Mechanical Force. *Proc. Natl. Acad. Sci. U. S. A.* **2003**, *100*, 1484−1489.
(11) Engler, A. J.; Sen, S.; Sweeney, H. L.; Discher, D. E. Matrix Elasticity Directs Stem Cell Lineage Specification. *Cell* **2006**, *126*, 677−689.
(12) Danilchik, M. V.; Brown, E. E.; Riegert, K. Intrinsic Chiral Properties of the Xenopus Egg Cortex: An Early Indicator of Left-Right Asymmetry? *Development* **2006**, *133*, 4517−4526.
(13) Lobikin, M.; Wang, G.; Xu, J. S.; Hsieh, Y. W.; Chuang, C. F.; Lemire, J. M.; Levin, M. Early, Nonciliary Role for Microtubule Proteins in Left-Right Patterning Is Conserved Across Kingdoms. *Proc. Natl. Acad. Sci. U. S. A.* **2012**, *109*, 12586−12591.
(14) Pohl, C.; Bao, Z. R. Chiral Forces Organize Left-Right Patterning in C. Elegans by Uncoupling Midline and Anteroposterior Axis. *Dev. Cell* **2010**, *19*, 402−412.
(15) Taniguchi, K.; Maeda, R.; Ando, T.; Okumura, T.; Nakazawa, N.; Hatori, R.; Nakamura, M.; Hozumi, S.; Fujiwara, H.; Matsuno, K. Chirality in Planar Cell Shape Contributes to Left-Right Asymmetric Epithelial Morphogenesis. *Science* **2011**, *333*, 339−341.
(16) Wan, L. Q.; Ronaldson, K.; Park, M.; Taylor, G.; Zhang, Y.; Gimble, J. M.; Vunjak-Novakovic, G. Micropatterned Mammalian Cells Exhibit Phenotype-Specific Left-Right Asymmetry. *Proc. Natl. Acad. Sci. U. S. A.* **2011**, *108*, 12295−12300.
(17) Chen, T.-H.; Hsu, J. J.; Zhao, X.; Guo, C.; Wong, M. N.; Huang, Y.; Li, Z.; Garfinkel, A.; Ho, C.-M.; Tintut, Y.; Demer, L. L. Left-Right Symmetry Breaking in Tissue Morphogenesis via Cytoskeletal Mechanics. *Circ. Res.* **2012**, *110*, 551−559.
(18) Singh, A. V.; Mehta, K. K.; Worley, K.; Dordick, J. S.; Kane, R. S.; Wan, L. Q. Carbon Nanotube-Induced Loss of Multicellular Chirality on Micropatterned Substrate Is Mediated by Oxidative Stress. *ACS Nano* **2014**, *8*, 2196−2205.
(19) Xu, J. S.; Van Keymeulen, A.; Wakida, N. M.; Carlton, P.; Berns, M. W.; Bourne, H. R. Polarity Reveals Intrinsic Cell Chirality. *Proc. Natl. Acad. Sci. U. S. A.* **2007**, *104*, 9296−9300.
(20) Tee, Y. H.; Shemesh, T.; Thiagarajan, V.; Hariadi, R. F.; Anderson, K. L.; Page, C.; Volkmann, N.; Hanein, D.; Sivaramakrishnan, S.; Kozlov, M. M.; Bershadsky, A. D. Cellular Chirality Arising from the Self-Organization of the Actin Cytoskeleton. *Nat. Cell Biol.* **2015**, *17*, 445−457.
(21) Mogilner, A.; Fogelson, B. Cytoskeletal Chirality: Swirling Cells Tell Left from Right. *Curr. Biol.* **2015**, *25*, R501−R503.
(22) Wang, G. L.; Manning, M. L.; Amack, J. D. Regional Cell Shape Changes Control Form and Function of Kupffer's Vesicle in the Zebrafish Embryo. *Dev. Biol.* **2012**, *370*, 52−62.
(23) Noël, E. S.; Verhoeven, M.; Lagendijk, A. K.; Tessadori, F.; Smith, K.; Choorapoikayil, S.; den Hertog, J.; Bakkers, J. A Nodal-Independent and Tissue-Intrinsic Mechanism Controls Heart-Looping Chirality. *Nat. Commun.* **2013**, *4*, 2754.
(24) Veerkamp, J.; Rudolph, F.; Cseresnyes, Z.; Priller, F.; Otten, C.; Renz, M.; Schaefer, L.; Abdelilah-Seyfried, S. Unilateral Dampening of Bmp Activity by Nodal Generates Cardiac Left-Right Asymmetry. *Dev. Cell* **2013**, *24*, 660−667.
(25) Hozumi, S.; Maeda, R.; Taniguchi, K.; Kanai, M.; Shirakabe, S.; Sasamura, T.; Spéder, P.; Noselli, S.; Aigaki, T.; Murakami, R.; Matsuno, K. An Unconventional Myosin in Drosophila Reverses the Default Handedness in Visceral Organs. *Nature* **2006**, *440*, 798−802.
(26) Spéder, P.; Adám, G.; Noselli, S. Type ID Unconventional Myosin Controls Left-Right Asymmetry in Drosophila. *Nature* **2006**, *440*, 803−807.
(27) Conti, M. A.; Adelstein, R. S. Nonmuscle Myosin II Moves in New Directions. *J. Cell Sci.* **2008**, *121*, 11−18.
(28) Maruthamuthu, V.; Sabass, B.; Schwarz, U. S.; Gardel, M. L. Cell-ECM Traction Force Modulates Endogenous Tension at Cell-Cell Contacts. *Proc. Natl. Acad. Sci. U. S. A.* **2011**, *108*, 4708−4713.
(29) Trepat, X.; Wasserman, M. R.; Angelini, T. E.; Millet, E.; Weitz, D. A.; Butler, J. P.; Fredberg, J. J. Physical Forces During Collective Cell Migration. *Nat. Phys.* **2009**, *5*, 426−430.
(30) Burton, K.; Taylor, D. L. Traction Forces of Cytokinesis Measured with Optically Modified Elastic Substrata. *Nature* **1997**, *385*, 450−454.
(31) Munevar, S.; Wang, Y. L.; Dembo, M. Traction Force Microscopy of Migrating Normal and H-ras Transformed 3T3 Fibroblasts. *Biophys. J.* **2001**, *80*, 1744−1757.
(32) Haase, K.; Pelling, A. E. Investigating Cell Mechanics with Atomic Force Microscopy. *J. R. Soc., Interface* **2015**, *12*, 20140970.
(33) Fung, A. O.; Kapadia, V.; Pierstorff, E.; Ho, D.; Chen, Y. Induction of Cell Death by Magnetic Actuation of Nickel Nanowires Internalized by Fibroblasts. *J. Phys. Chem. C* **2008**, *112*, 15085−15088.
(34) Gao, N.; Wang, H. J.; Yang, E. H. An Experimental Study on Ferromagnetic Nickel Nanowires Functionalized with Antibodies for Cell Separation. *Nanotechnology* **2010**, *21*, 105−107.
(35) Hultgren, A.; Tanase, M.; Chen, C. S.; Meyer, G. J.; Reich, D. H. Cell Manipulation Using Magnetic Nanowires. *J. Appl. Phys.* **2003**, *93*, 7554−7556.
(36) Hultgren, A.; Tanase, M.; Felton, E. J.; Bhadriraju, K.; Salem, A. K.; Chen, C. S.; Reich, D. H. Optimization of Yield in Magnetic Cell Separations Using Nickel Nanowires of Different Lengths. *Biotechnol. Prog.* **2005**, *21*, 509−515.
(37) Zhang, L.; Petit, T.; Peyer, K. E.; Nelson, B. J. Targeted Cargo Delivery Using a Rotating Nickel Nanowire. *Nanomedicine* **2012**, *8*, 1074−1080.
(38) Murrell, M.; Oakes, P. W.; Lenz, M.; Gardel, M. L. Forcing Cells into Shape: The Mechanics of Actomyosin Contractility. *Nat. Rev. Mol. Cell Biol.* **2015**, *16*, 486−498.
(39) Hotulainen, P.; Lappalainen, P. Stress Fibers Are Generated by Two Distinct Actin Assembly Mechanisms in Motile Cells. *J. Cell Biol.* **2006**, *173*, 383−394.
(40) Tojkander, S.; Gateva, G.; Lappalainen, P. Actin Stress Fibers - Assembly, Dynamics and Biological Roles. *J. Cell Sci.* **2012**, *125*, 1855−1864.
(41) Hossain, M. Z.; Kleve, M. G. Nickel Nanowires Induced and Reactive Oxygen Species Mediated Apoptosis in Human Pancreatic Adenocarcinoma Cells. *Int. J. Nanomed.* **2011**, *6*, 1475−1485.
(42) Worley, K. E.; Shieh, D.; Wan, L. Q. Inhibition of Cell-Cell Adhesion Impairs Directional Epithelial Migration on Micropatterned Surfaces. *Integr. Biol.* **2015**, *7*, 580−590.
(43) Pan, H.; Liu, B. H.; Yi, J. B.; Poh, C.; Lim, S.; Ding, J.; Feng, Y. P.; Huan, C. H. A.; Lin, J. Y. Growth of Single-Crystalline Ni and Co Nanowires via Electrochemical Deposition and Their Magnetic Properties. *J. Phys. Chem. B* **2005**, *109*, 3094−3098.
(44) Pan, H.; Sun, H.; Poh, C.; Feng, Y. P.; Lin, J. Y. Single-Crystal Growth of Metallic Nanowires with Preferred Orientation. *Nanotechnology* **2005**, *16*, 1559−1564.
(45) Thongmee, S.; Pang, H. L.; Ding, J.; Lin, J. Y. Fabrication and Magnetic Properties of Metallic Nanowires via AAO Templates. *J. Magn. Magn. Mater.* **2009**, *321*, 2712−2716.
(46) Ruoslahti, E. Fibronectin in Cell Adhesion and Invasion. *Cancer Metastasis Rev.* **1984**, *3*, 43−51.
(47) Tan, J. L.; Liu, W.; Nelson, C. M.; Raghavan, S.; Chen, C. S. Simple Approach to Micropattern Cells on Common Culture Substrates by Tuning Substrate Wettability. *Tissue Eng.* **2004**, *10*, 865−872.

DOI: 10.1021/acsnano.6b01142
ACS Nano 2016, 10, 7409−7417